Proceedings of The Canadian Society for Mechanical Engineering International Congress 2018
CSME International Congress 2018
May 27-30, 2018, Toronto, On, Canada

DISPLACEMENT FLOWS OF VISCOPLASTIC FLUIDS IN NEAR-HORIZONTAL CHANNELS: NUMERICAL AND ANALYTICAL SIMULATIONS

Ali Eslami, Roozbeh Mollaabbasi, Seyed Mohammad Taghavi
Department of Chemical Engineering, Laval University, Quebec, QC, Canada
Seyed-Mohammad.Taghavi@gch.ulaval.ca

Abstract-The miscible displacement flow of a viscoplastic fluid by a Newtonian fluid is studied numerically and analytically in a near-horizontal 2D channel. We focus on a density-unstable flow configuration where the displacing fluid is heavier than the displaced one with a laminar imposed flow. Using numerical and analytical approaches, we demonstrate that the channel inclination has the significant impacts on the viscoplastic flow morphology and front height. In addition, we study the yield stress impacts on the viscoplastic flow features.

Keywords-Displacement flow; viscoplastic fluid; inclination impacts, numerical and analytical approaches

I. Introduction

Many industrial processes require the cleaning and removal of a gelled-like material (i.e., typically viscoplastic) from a duct. For example, it can be mentioned oil & gas well cementing, waxy crude oil pipeline restarts, gas-assisted injection molding, biomedical applications (mucus, biofilms), cleaning of equipment and environmental surfaces, and food processing [2]. An import issue in these processes is the existence of the residual deposits. The aforementioned processes may have different fluid properties (e.g., different densities/viscosities and miscible/immiscible liquids) and flow geometries (e.g., pipe, annulus, channel). In this study, we numerically and analytically consider buoyant miscible, iso-viscous displacement flows of a viscoplastic fluid (displaced fluid) by a Newtonian one (displacing fluid) in a plane channel where the imposed flow is laminar.

Previously, we have investigated the impacts of three dimensionless numbers (i.e., the Bingham number, the densimetric Froude number and the Reynolds number) on the displacement of a viscoplastic fluid by a Newtonian fluid of higher density numerically [1] and analytically [4]; which covered various buoyancy effects from very small to very large Froude numbers. For brevity, we refer to these papers for a more detailed introduction and review of previous works. The main finding in the previous works was that the yield stress can lead to appear various flow regimes and have a significant effect on the displacing fluid front profile and residual layer thickness. The novelty of the current work is in studying impacts of channel inclination on the viscoplastic displacement flows at very small Froude number, through numerical and analytical approaches, which have not been studied so far.

II. Governing Equations

In this study the miscible displacement flow of a Bingham fluid (light fluid) by a Newtonian one (heavy fluid) along a channel is studied. These fluids have the same viscosity whereas their density are different. We choose Cartesian coordinates $(\hat{x}, \hat{y})$ with $\hat{x}$ representing the streamwise direction.[1] The flow geometry and notation used in the current study is represented in Fig. 1. The governing dimensionless equations of motion are:

$$[1 + \phi At]Re \left[\frac{\partial}{\partial t}\mathbf{u} + (\mathbf{u}.\nabla)\,\mathbf{u}\right] = \tag{1}$$

[1] In this paper, we adopt the convention of denoting dimensional quantities with the ˆ symbol and dimensionless quantities without.

$$-\nabla p + \nabla.\tau + \frac{\phi Re}{Fr^2}\mathbf{e}_g,$$

$$\nabla.\mathbf{u} = 0, \quad (2)$$

$$C_t + \mathbf{u}\cdot\nabla C = \frac{1}{Pe}\nabla^2 C, \quad (3)$$

where p, $\mathbf{u}$ and τ are the pressure, the velocity and the deviatoric stress. Here $\mathbf{e}_g = (\cos\beta, -\sin\beta)$ and the function $\phi(C) = 2C - 1$ interpolates linearly between -1 and 1 for $C \in [0, 1]$. No slip conditions are satisfied at the walls, the heavy fluid enters fully developed (plane Poiseuille profile) at $x = -L/4$ (inlet) and outflow conditions are applied at $x = 3L/4$ (outlet).

Five dimensionless numbers appear in (1-3) including: the Reynolds number $Re = \frac{\hat{V}_0\hat{D}}{\hat{\nu}}$ (here $\hat{D}$ is the channel width), Péclet number $Pe = \frac{\hat{V}_0\hat{D}}{\hat{D}_m}$ (here $\hat{D}_m$ is the molecular diffusivity), densimetric Froude number $Fr = \frac{\hat{V}_0}{\sqrt{At\hat{g}\hat{D}}}$, channel inclination β, Atwood number $At = \frac{(\hat{\rho}_H - \hat{\rho}_L)}{(\hat{\rho}_H + \hat{\rho}_L)}$ which represents a dimensionless density difference, where $\hat{\rho}_H$ and $\hat{\rho}_L$ are the density of Newtonian fluid and Bingham fluid, respectively. Since $\hat{\rho}_H > \hat{\rho}_L$ (i.e., the heavy fluid displaces the light fluid), $At > 0$ in this paper. It should be mentioned that displacement flows with small density differences were considered, for which the Boussinesq approximation is implemented. The density differences can remarkably affect buoyancy effects, captured by the densimetric Froude number. Finally, $Pe \gg 1$ which means that on the timescale of interest, $\hat{D}_m$ does not play a major role in the flows studied.

The constitutive laws for Newtonian fluid (displacing fluid) is $\tau(\mathbf{u}) = \dot{\gamma}(\mathbf{u})$ with $\dot{\gamma} = \nabla\mathbf{u} + (\nabla\mathbf{u})^T$ and for the Bingham fluid (displaced fluid) which includes a yield stress is:

$$\tau_2(\mathbf{u}) = \left[1 + \frac{Bn}{\dot{\gamma}(\mathbf{u})}\right]\dot{\gamma}(\mathbf{u}) \Leftrightarrow \tau_2(\mathbf{u}) > Bn, \quad (4)$$

$$\dot{\gamma}(\mathbf{u}) = 0 \Leftrightarrow \tau_2(\mathbf{u}) \leq Bn, \quad (5)$$

where the second invariants ($\dot{\gamma}(\mathbf{u})$) and $\tau_2(\mathbf{u})$, are defined by:

$$\dot{\gamma}(\mathbf{u}) = \left[\frac{1}{2}\sum_{i,j=1}^{2}[\dot{\gamma}_{ij}(\mathbf{u})]^2\right]^{1/2},$$

$$\tau_2(\mathbf{u}) = \left[\frac{1}{2}\sum_{i,j=1}^{2}[\tau_{2,ij}(\mathbf{u})]^2\right]^{1/2}, \quad (6)$$

where Bn is the Bingham number: $Bn \equiv \frac{\hat{\tau}_Y}{\hat{\mu}_1[\hat{V}_0/\hat{D}_0]}$.

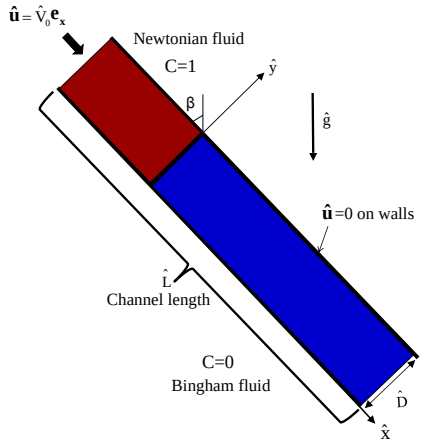

Figure 1: Schematic view of the numerical domain and initial flow configuration.

III. Computational Method

The equations of motion was discretized using a mixed finite element-finite volume method, using the classical augmented Lagrangian method of [3] to resolve unyielded zones. More details of the numerical approach are described in [5]. The present numerical algorithm was implemented in C++ and solved using an open source platform, PELICANS. More details about employing this platform for numerical simulation of displacement flow are given in [6].

In the current simulation study, 63,000 mesh cells (1500×42) were used for all simulations while the meshes (regular rectangular) in the y-direction were refined slightly towards the channel walls. The initial interface between the two fluids was placed at distance $L/4$ from the channel inlet in the computational domain which means that at $t = 0$, the two fluids are separated by an imaginary gate valve located at $x = 0$. It is worth noting that the dependency of results on the mesh size have been examined and also the results are validated which shows a great agreement with the previous model [1]. Note that the computational cost is high.

IV. Analytical Method

In this part, a lubrication approximation model is developed to simplify the governing displacement flow equations and propose a semi-analytical solution for the heavy and light fluid flux functions to reduce the computational cost. Therefore, we scale our equations using a dimensionless length-scale, $\delta^{-1} \gg 1$, over which the interface elongates. We assume that δ has a size of $\hat{D}/\hat{L}$, in which $\hat{L}$ denotes the characteristic spreading length of the interface. Defining $\delta x = X$, $\delta t = T$, $\delta p = P$, $v = \delta V$ and following standard methods, we can now re-scale our equations to (assume that

$\delta \to 0$ with fixed Re):

$$0 = -\frac{\partial P}{\partial X} + \frac{\partial}{\partial y}\tau_{k,Xy} + \frac{\partial}{\partial z}\tau_{k,Xz} \pm \frac{\chi}{2}, \quad (7)$$

$$0 = -\frac{\partial P}{\partial y} \mp \delta\frac{\chi}{2}\tan\beta, \quad (8)$$

$$0 = -\frac{\partial P}{\partial z}, \quad (9)$$

where $\chi = \frac{2Re\cos\beta}{Fr^2}$. The interface is advected via a kinematic condition furnishing the dependence of the velocity on space and time:

$$\frac{\partial h}{\partial T} + u\frac{\partial h}{\partial X} = V. \quad (10)$$

Combining the incompressibility condition with the kinematic condition results in

$$\frac{\partial h}{\partial T} + \frac{\partial q}{\partial X} = 0, \quad (11)$$

where q is defined as:

$$q = \int_0^h u dy. \quad (12)$$

V. Results

In this section the computational results are presented. In a typical simulation, as time progresses, due to the imposed velocity, the heavy fluid layer penetrates into the light fluid layer and displaces it. Through the displacement flow process, different interesting flow patterns are formed at the interface between fluids.

Figure 2 shows the concentration maps of the numerical simulation as time evolves, run for $Re = 400$ and $Fr = 0.9$. The yield stress in the horizontal channel ($\beta = 90°$) for the Fig. 2a and Fig. 2b is different such that the yield stress for Fig. 2a is zero ($Bn = 0$, Newtonian fluid) while for the Fig. 2b is considerable ($Bn = 0$, Bingham fluid). A nearly symmetric displacement flow is observed in Fig. 2a and the displacing finger is similar to a Poiseuille-like profile. At $Bn = 10$, the displacement flow remains symmetric and the front shape is similar to a plug-like profile (see Fig. 2b). The only difference between the Fig. 2b (horizontal channel) and Fig. 2c ($\beta = 88°$) is that the channel is more inclined with respect to vertical in the latter. Figure 2b shows a qualitatively stable flow while in the Fig. 2c the yield stress of the displaced fluid has not been able to damp interfacial instabilities due to channel inclination.

Figure 3 presents examples of our simulations, for $\beta = 80°$, $Bn = 50$, $Re = 400$ and $Fr = 0.9$ at given time. Initially at $x = 0$, the Newtonian fluid and Bingham one are completely separated. However, as time progresses, impacts of the imposed flow and the density ratio, leads to penetration of the heavy fluid through the light fluid and

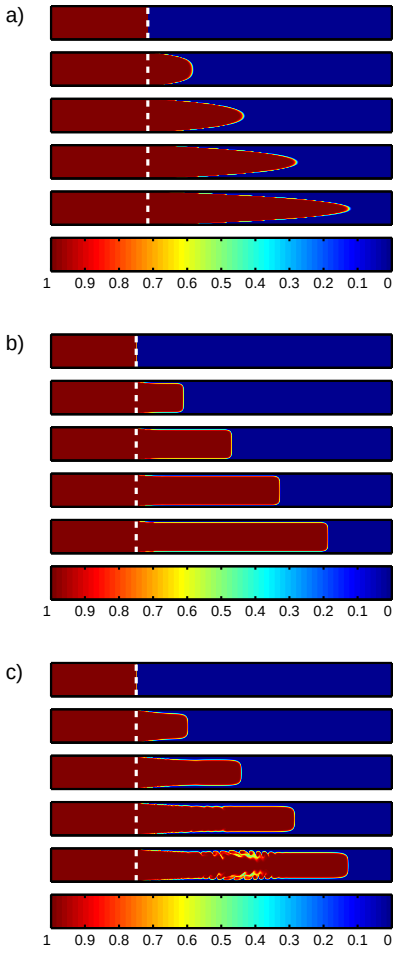

Figure 2: Concentration colormaps of the displacement flow at times $t = [0, 8.75, ..., 35]$ for $Re = 400$ and $Fr = 0.9$; a) $Bn = 0$ and $\beta = 90°$. b) $Bn = 10$ and $\beta = 90°$. c) $Bn = 10$ and $\beta = 88°$. The last image at the bottom of each subfigure is the colorbar of the concentration values. The white broken lines display the position of the initial interface $x = 0$ (gate valve). The domain size shown is 1×100.

attempts to sweeps it. Figure. 3a depicts the concentration colormap of the displacement flow such that at longer spatial position with respect to the initial gate valve, the displaced layers adjacent to the walls become apparently static. Furthermore, it can be observed that the displacement flow is stable over a long time. The shear stress colormaps at the same time as the colormap of concentration is plotted in Fig. 3b, confirming that the stress field asymmetry results in asymmetric static layers on the top/bottom walls. Figure 3c displays the speed contours, $V = \sqrt{{V_x}^2 + {V_y}^2}$, at the same simulation parameters as in Fig. 3a, where V_x and V_y are the stream-wise and depthwise velocity components, respectively. A Poiseuille profile is observed before

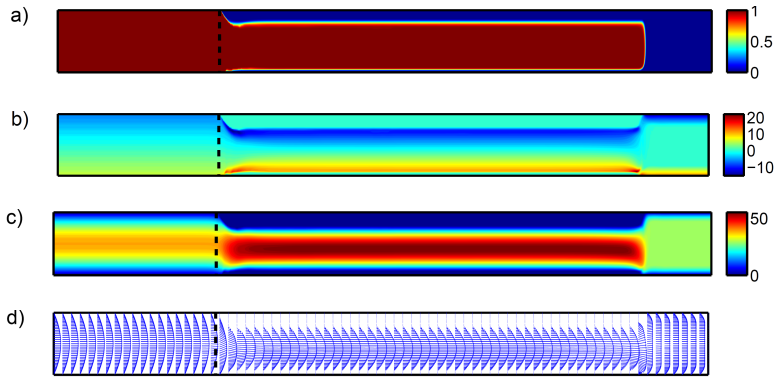

Figure 3: Computational results for $Bn = 50$, $Re = 400$ and $Fr = 0.9$ and $\beta = 80^\circ$ at time $t = 34$: a) Concentration colormap; b) Shear stress colormap; c) Speed contours: $V = \sqrt{{V_x}^2 + {V_y}^2}$. d) Velocity vectors. The black broken lines display the position of the initial interface $x = 0$.

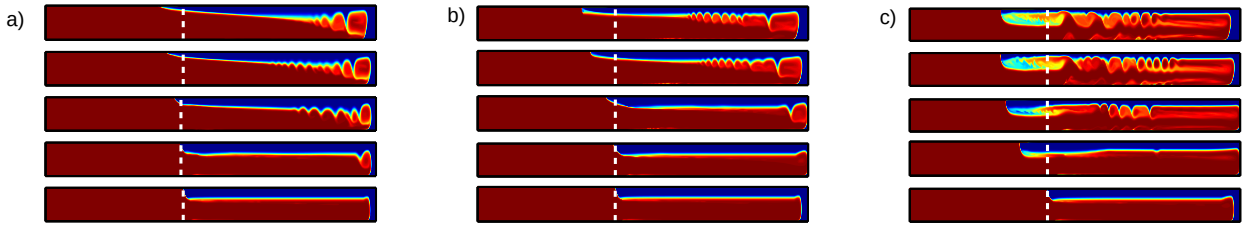

Figure 4: Panorama of concentration colormaps at $t = 16$, $Fr = 0.5$ and $Re = 400$ for a) $\beta = 90^\circ$, b) $\beta = 88^\circ$ and c) $\beta = 82^\circ$. The rows from top to bottom show $Bn = 0$, $Bn = 5$, $Bn = 20$, $Bn = 50$, $Bn = 100$. The domain size shown is 1×60.

the gate valve location such that the high-speed regions remain towards the channel center. However, the speed contours are zero within the displaced fluid layers adjacent the upper and lower walls after the gate valve, which means that the remaining displaced layers are completely static. Figure 3d shows the velocity vector fields along the channel length. This graph confirms that the flow is nearly stable and that the displaced fluid layer close to top wall is entirely static. It can be observed that the fluid within the displaced layer has a zero velocity.

The effects of yield stress value and channel inclination for $Re = 400$ and $Fr = 0.5$ are presented in Fig. 4. Figure 4a, b and c show panoramas of the concentration colormaps at $t = 16$ for $\beta = 90^\circ$, $\beta = 88^\circ$ and $\beta = 82^\circ$, respectively. As seen, for a given channel inclination, by increasing the dimensionless yield stress, the flow morphology changes remarkably. For example, at $\beta = 88^\circ$, the interfacial instabilities decrease by increasing the Bingham number such that the yield stress can damp the interfacial waves. Moreover, the trailing front has an indirect relation with Bn. In other words, at small yield stress the trailing front moves upwards, while at larger Bingham number, the moving of the trailing front completely stops. It also can be seen, at fixed Bn, by increasing the channel inclination the flow becomes more unstable and trailing front shows different behavior. Finally, it can be conclude that from Fig. 4 and Fig. 2, at large Froude number, the displacement flow is nearly symmetric which means that the displacing fluid moves more or less along the center of the channel. However, at small Fr, the displacement flow is asymmetric; displacing finger advances approximately near the lower wall of the channel.

The analytical results are presented in Fig. 5 and Fig. 6. Figure 5 shows the dependency of the displacing front height to yield stress. By increasing the yield stress of displacing fluid the front hight decreases and the static layer increases.

Figure 6 shows the effect of increasing the buoyancy force (χ) in the heavy-light fluids displacement. Increasing the inclination of the channel reinforces the buoyancy force therefore, the buoyancy overcomes the yield stress and the back flow is observed in Fig. 6c. Our results show that the analytical approach is also generally able to predict the variation of flow morphology with yield stress and channel inclination in the viscoplastic fluid displacement with low computational cost.

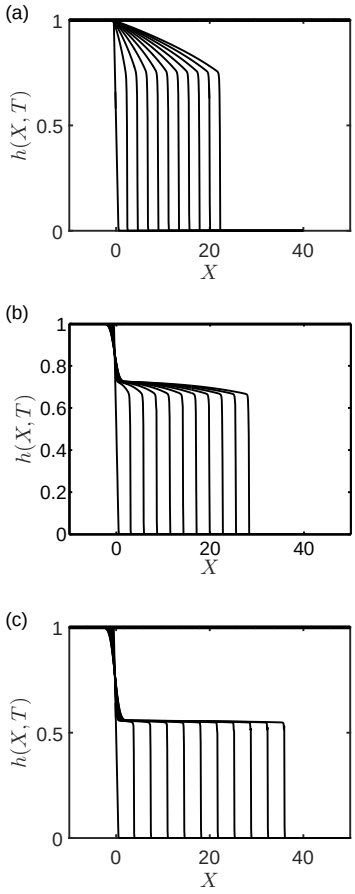

Figure 5: Interface evolution in time, T = 0, 2, ..., 18, 20. β, Fr and Re are 90^o, 0.5 and 400 respectively in all figures. Bn number is 0, 5 and 50 from up to down. The displacing fluid is Newtonian.

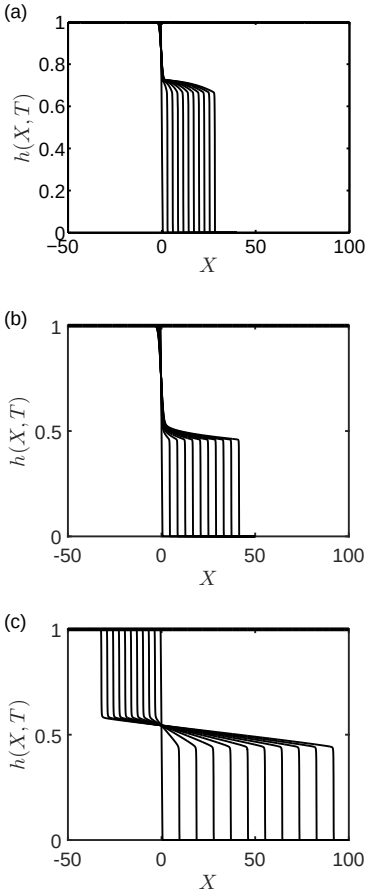

Figure 6: Interface evolution in time, T = 0, 2, ..., 18, 20. Bn, Fr and Re are 20, 0.5 and 400 respectively in all figures. β is 90^o, 88^o and 82^o from up to down. The displacing fluid is Newtonian.

VI. Conclusion

In this study, we have numerically and analytically considered a fascinating displacement flow where the heavier displacing fluid (Newtonian fluid) pushes the lighter displaced fluid (viscoplastic fluid) along a 2D plane channel. During the miscible displacement flow, the results demonstrate that the variation of channel inclination and yield stress has the remarkable impacts on the flow morphology. Also the results show that the yield stress (at larger Bingham number) damps the interfacial instabilities. The viscoplastic displacement flows, at given Bn, for more channel inclination can be more unstable.

References

[1] A. Eslami, I.A. Frigaard, and S.M. Taghavi. Viscoplastic fluid displacement flows in horizontal channels: Numerical simulations. *J. non-Newt. Fluid Mech.*, 249:79–96, 2017.

[2] A. Eslami and S.M. Taghavi. Viscous fingering regimes in elasto-visco-plastic fluids. *J. non-Newt. Fluid Mech.*, 243:79–94, 2017.

[3] R. Glowinski and P. Le Tallec. Augmented Lagrangian and operator-splitting methods in nonlinear mechanics. *Phys. Fluids*, 19:084106, 2007.

[4] R. Mollaabbasi and S.M. Taghavi. Buoyant displacement flows in slightly non-uniform channels. *J. Fluid Mech.*, 795:876–913, 2016.

[5] A. Roustaei. *Yield stress fluid flows in uneven geometries: applications to the oil and gas industry*. PhD thesis, University of British Columbia, 2016.

[6] S.M. Taghavi, T. Séon, K. Wielage-Burchard, D.M. Martinez, and I.A. Frigaard. Stationary residual layers in buoyant Newtonian displacement flows. *Phys. Fluids*, 23(4):044105, 2011.